

Ultracold-atom quantum simulator for attosecond science

Simon Sala, Johann Förster, and Alejandro Saenz

AG Moderne Optik, Institut für Physik, Humboldt-Universität zu Berlin, Newtonstraße 15, 12489 Berlin, Germany

(Dated: November 6, 2018)

A quantum simulator based on ultracold optically trapped atoms for simulating the physics of atoms and molecules in ultrashort intense laser fields is introduced. The slowing down by about 13 orders of magnitude allows to watch in slow motion the tunneling and recollision processes that form the heart of attosecond science. The extreme flexibility of the simulator promises a deeper understanding of strong-field physics, especially for many-body systems beyond the reach of classical computers. The quantum simulator can experimentally straightforwardly be realized and is shown to recover the ionization characteristics of atoms in the different regimes of laser-matter interaction.

In his renowned lecture, “Simulating physics with computers” [1] Richard P. Feynman suggested the use of quantum simulators, i.e. precisely controllable quantum systems, to simulate other quantum systems that cannot be described theoretically due to their exponentially growing Hilbert space. For instance, the Mott-insulator to superfluid phase transition in condensed-matter systems [2] was predicted [3] to be observable with ultracold atoms in an optical lattice and then successfully demonstrated [4, 5]. Also the Higgs mechanism [6], high temperature superconductivity [7], or *Zitterbewegung* [8] (to name just a few) were successfully investigated by quantum simulation. Moreover, the quantum simulation of electrons in crystalline solids exposed to laser fields [9] has been proposed.

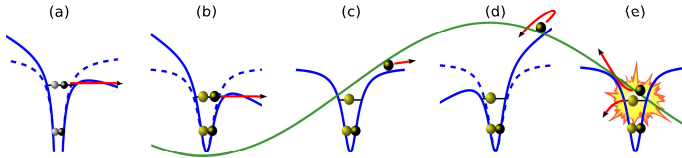


Figure 1. (color online) **(a) & (b)**: Comparison of electrons in an atom exposed to a strong electric field (a) and atoms in an optical trap exposed to a magnetic-field gradient (b). The different shadings of the electrons and atoms reflects their different spin states and Zeeman substates, respectively. An external electric field (a) or magnetic-field gradient (b) effectively tilts the continuum threshold and the electrons (a) or atoms (b) can escape the binding potential by tunneling. **(b) - (e)**: Behavior of optically trapped atoms in a periodically driven magnetic-field gradient (solid green curve), as expected from the three-step model [10] in strong-field physics. After tunneling (b) the escaped atom accelerates (c), reverses (d) and finally recollides (e) with the residual atoms.

Strong-field physics has contributed considerably to the understanding of the light-matter interaction. The progress leading to pulses on the attosecond timescale [11] has even raised visions of real-time imaging of molecular processes [12] and orbital tomography [13]. Yet, attosecond many-body physics is challenging. An exact investigation on classical computers beyond the single-active-electron approximation becomes prohibitively complex for many-electron systems. In fact,

the numerical treatment of two-electron systems like He or H_2 is today still state of the art [14–17]. Thus, simplified models are widely used for interpreting modern experiments. These models are controversial and their validation is difficult for several reasons. First, the used light pulses are bound to the specifications of the laser. The wavelength range of lasers is limited, mostly Ti:sapphire lasers are used. The pulse shapes are restricted and can often only be reproduced and determined up to a considerable uncertainty. The intensity and timescale of laser pulses are already pushed to a limit where further improvements require major technical or even principle developments with new limitations, like free-electron lasers. Second, atoms, ions, and molecules are complicated many-body systems. Their internal structure cannot be simply manipulated. For example, a variation of the number of electrons or protons underlies constraints due to electroneutrality. Third, although the correlation of electronic and nuclear motion is known to influence the ionization behavior [18, 19], in most theoretical models this effect is neglected by fixing the nuclei in space while investigating the electronic response to the laser field.

In this work, we introduce the concept of an ultracold-atom quantum simulator for attosecond science which offers great flexibility and control beyond the mentioned limitations. This includes many-body quantum simulations that are impossible with any classical computer.

The attoscience simulator. The simulator system consists of ultracold trapped atoms that replace the electrons in the atom, ion, or molecule, see Fig. 1. The core potential is replaced by an external, optical trapping potential. The ability to implement single-well or multi-well trapping potentials allows for a simulation of atoms or molecules, respectively. Naturally, fermionic atoms may be chosen, but using bosons or distinguishable particles reveals effects of the exchange interaction. The intense laser pulse is replaced by a periodically driven magnetic-field gradient which is generated by current-carrying coils. Restrictions for ultrashort laser fields like the zero-net-force condition [20] do not apply here and thus fields of almost arbitrary shape can be created, even true half-cycle pulses and fields that formally correspond to sub-attosecond pulses.

Certainly, the atom-atom interaction is shorter ranged than the Coulomb interaction. However, earlier quantum simulations like the famous superfluid to Mott-insulator phase transition [3] demonstrated that an equivalent physics is obtainable. The use of ultracold atoms introduces the unique opportunity to arbitrarily vary the effective interaction strength *via* magnetic Feshbach resonances. This promises new insights on the influence of the interparticle interaction on the ionization behavior. Furthermore, theoretical studies which replace the core potential by, e.g., a zero-range potential [20], can now be tested experimentally, and this even for many-particle systems. Since ultracold quantum systems are manipulated nowadays on the single-atom level [21, 22], important tests of the widely used single-active-electron approximation and a detailed investigation of correlated many-body tunneling become accessible. Moreover, only the simulator allows for the experimental realization of fixed nuclei – a task impossible with real molecules due to the Heisenberg uncertainty principle. The influence of a fixed nuclear geometry on the ionization behavior [23] can thus be tested experimentally in a clean fashion. Additionally, the differences between the quantum-mechanical nature of vibronic states and the simulation of a mechanical vibration of the nuclei can be investigated.

Hamiltonian mapping. The formal equivalence of the quantum simulator Hamiltonian to the electronic strong-field Hamiltonian at a fixed nuclear configuration is demonstrated. When treating the strong laser field classically, which is acceptable due to its high intensity, and applying dipole approximation and length gauge (LG), respectively, the electronic strong-field Hamiltonian reads

$$\hat{H}^{\text{LG}}(t) = \hat{H}_0 + \sum_{i=1}^N \mathbf{r}_i \cdot e\mathbf{E}(t) \quad , \quad (1)$$

where

$$\hat{H}_0 = \sum_{i=1}^N \frac{\hat{\mathbf{p}}_i^2}{2m_e} + V_{\text{ee}} + V_{\text{e,nuc}} \quad (2)$$

denotes the field-free Hamiltonian for N electrons. m_e is the electron mass, e the electron charge, V_{ee} includes all electron-electron repulsion terms, and $V_{\text{e,nuc}}$ all the electron-nucleus interactions. \mathbf{E} denotes the electric-field component of the pulse. In analogy, the Hamiltonian of N ultracold atoms confined in a trapping potential $\mathcal{V}_{\text{a,tr}}$ which are exposed to a time-dependent magnetic-field gradient $\mathcal{B}'(t)$ reads

$$\hat{\mathcal{H}}^{\text{LG}}(t) = \hat{\mathcal{H}}_0 + \sum_{i=1}^N \mathbf{r}_i \cdot \mu\mathcal{B}'(t) \quad , \quad (3)$$

where

$$\hat{\mathcal{H}}_0 = \sum_{i=1}^N \frac{\hat{\mathbf{p}}_i^2}{2m_a} + \mathcal{V}_{\text{aa}} + \mathcal{V}_{\text{a,tr}} \quad (4)$$

denotes the Hamiltonian of the atoms in the trap without the gradient \mathcal{B}' . m_a denotes the atomic mass, μ the magnetic moment of the atoms, \mathcal{V}_{aa} includes all atom-atom and $\mathcal{V}_{\text{a,tr}}$ all atom-trap interactions, respectively.

The Hamiltonians (1) and (3) are *formally* equivalent under the mapping

$$e\mathbf{E} \mapsto \mu\mathcal{B}' \quad . \quad (5)$$

It is important to note that the electro-dynamical potentials, e.g., the vector potential $-\frac{\partial\mathbf{A}(t)}{\partial t} = \mathbf{E}$, map accordingly. In the ultracold simulator system the “vector potential” is thus given by

$$-\frac{\partial\mathcal{A}(t)}{\partial t} = \mathcal{B}' \quad . \quad (6)$$

Of course, the potential \mathcal{A} differs from the physical vector potential $\tilde{\mathbf{A}}$ that generates the magnetic field \mathcal{B} and its gradient \mathcal{B}' via $\mathcal{B} = \nabla \times \tilde{\mathbf{A}}$. Yet, equation (6) is the formal consequence of the simulator mapping (5).

The simulator mapping (5) is intrinsically defined in length gauge. However, it is particularly useful to consider the analog of the velocity-gauge (VG) formulation, too. A gauge transformation of the strong-field Hamiltonian (1) leads to the velocity-gauge form

$$\hat{H}^{\text{VG}}(t) = \hat{H}_0 + \sum_{i=1}^N \frac{e}{m_e} \mathbf{A}(t) \cdot \hat{\mathbf{p}}_i + \frac{e^2}{2m_e} \mathbf{A}(t)^2 \quad (7)$$

In analogy, a “gauge” transformation of the simulator Hamiltonian (3) leads to the corresponding simulator Hamiltonian in “velocity gauge”,

$$\hat{\mathcal{H}}^{\text{VG}}(t) = \hat{\mathcal{H}}_0 + \sum_{i=1}^N \frac{\mu}{m_a} \mathcal{A}(t) \cdot \hat{\mathbf{p}}_i + \frac{\mu^2}{2m_a} \mathcal{A}(t)^2 \quad . \quad (8)$$

Again, the Hamiltonians are *formally* equivalent. The vector potential $\mathcal{A}(t)$ is the one resulting from the simulator mappings (5) and (6).

Experimental realization. As a possible realization we consider the experiment of the group of Selim Jochim [21] where a well defined number of fermionic atoms can be loaded into a tight optical dipole trap in a well defined quantum state. This trap is in good approximation described by a one-dimensional Lorentz potential [24]. A *static* magnetic-field gradient which tilts the continuum threshold of the trap, see Fig. 1, is applied for the preparation and investigation of the system. The here proposed attoscience quantum simulator is realized by replacing the static magnetic-field gradient by a periodically driven one.

Similarly to strong-field physics, the pulse may be defined by its vector potential *via*

$$\mathcal{A}(t) = \mathcal{A}_0 \sin\left(\frac{\omega t}{2n_c}\right)^2 \sin(\omega t + \varphi) \quad . \quad (9)$$

Here, n_c is the number of cycles, $\varphi = 0$ is the carrier-envelope phase, ω the angular frequency, and \mathcal{A}_0 from which \mathcal{B}'_0 is obtained *via* equation (6) is the strength of the perturbation. For a given simulator setup and a specific pulse, the corresponding values for the frequency ω_e and peak vector potential $|\mathcal{A}_0|$ applied in the strong-field system are found by enforcing equal Keldysh parameters [10, 25] and an equal ratio of the binding energy to the frequency of the perturbing field [24].

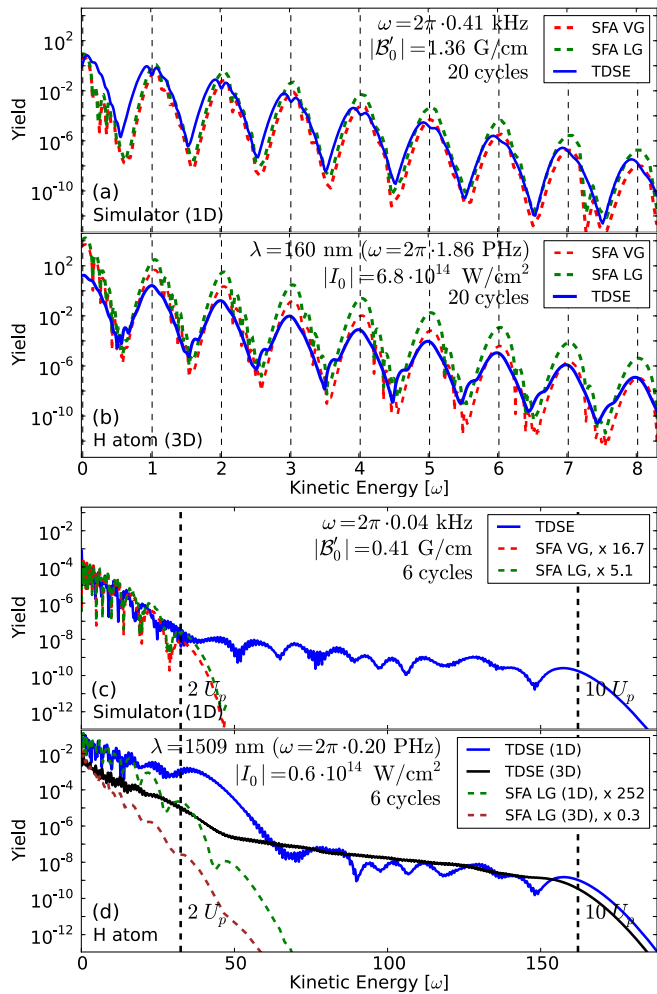


Figure 2. (color online) Atom spectra of the simulator and electron spectra of a hydrogen atom for the multiphoton regime, (a) and (b) respectively, and for the quasistatic regime, (c) and (d) respectively. The dashed vertical lines in (a) and (b) indicate the positions of the multiphoton peaks for an infinitely long pulse as expected from the subsequent absorption of field quanta. In (d), in addition to the result for the hydrogen atom in three dimensions, also the result for the one-dimensional (1D) *soft-Coulomb* potential $V(z) = -1/\sqrt{2+z^2}$ is shown. The SFA yields in (c) and (d) are rescaled in order to agree with the total ionization yield of the TDSE calculation. The factors are given in the figure legends.

Validation of the quantum simulator. In the experi-

ment [21] the simulator builds on, the atom loss is routinely measured. This observable corresponds to a measurement of the total ion (or electron) yield in a strong-field experiment. More detailed information on the underlying physics is obtained by a measurement of differential yields: energy-resolved electron or atom spectra for strong-field experiments or the simulator, respectively. The measurement of energy-resolved atom spectra requires further experimental developments, similarly to strong-field physics where in the early days also only total yields were measured. To validate the simulator in more detail, energy-resolved electron spectra of a hydrogen atom are compared to the corresponding energy-resolved atom spectra of the simulator setup, both initially in their ground state. The spectra are calculated by solving the corresponding time-dependent Schrödinger equations (TDSE) [24], ensuring that the corresponding parameters for the quantum simulator are experimentally accessible [26].

The laser-matter interaction is typically divided into two characteristic regimes. In the low-frequency, high-intensity regime the system is assumed to follow adiabatically the changes of the electric field of the laser. In this quasistatic regime the electron is supposed to tunnel through or escape over the field-distorted potential barrier, see Fig. 1. In the other limit of the high-frequency, low-intensity regime the multiphoton picture is usually adopted in which the ionization is described within a simplified picture as an absorption of photons, despite the fact that in the theoretical treatment the electromagnetic field is treated classically.

In the multiphoton regime (Figs. 2a and b), both spectra show the typical multi-peak structure (above-threshold-ionization peaks) where the peak distance reflects the frequency of the perturbing field. Clearly, simulator and hydrogen atom show very good agreement. Despite the different dimensionalities the TDSE solutions agree, in fact, almost quantitatively.

In the quasistatic regime (Figs. 2c and d), a simple tunneling picture suggests an exponential decrease in the energy-resolved spectra, as is seen in the low-energy part (up to $2U_p$ where $U_p = I/(4\omega^2)$ is the ponderomotive energy and I the laser intensity). However, in a periodically changing field the emitted electron or atom can reverse its direction of motion and recollide, see Fig. 1. High-harmonic generation in strong-field physics is based on the recombination of the liberated electron with the parent ion at the recollision step. Using classical Newtonian mechanics it had been found that high-harmonic spectra extend up to $3.17U_p + I_p$ [27]. For energy resolved electron spectra, the recollision process leads to a broad energy distribution of the rescattered electrons which manifests in a plateau as observed in [28] and clearly seen in Fig. 2d. In analogy to the high-harmonic cutoff law classical Newtonian mechanics predicts an extension of this plateau between $2U_p$ and $10U_p$ [29]. Clearly, the sim-

ulator shows all expected features, both from tunneling and rescattering. However, the more pronounced structures in the plateaus of the 1D systems (simulator and 1D hydrogen atom) reveal effects of the dimensionality. Such effects can be studied with the simulator even experimentally by varying the anisotropy of the trap – a task impossible in strong-field experiments.

Rescattering is the origin of nonsequential double ionization, high-energy above-threshold ionization, and high-order harmonic generation. A controlled recollision, see Fig. 1, of an escaped atom on residual bound atoms prepared in a specific configuration with variable interaction strength can reveal insights into correlated recollision dynamics relevant, e. g., for high harmonics [30] and non-sequential double ionization [31]. On the other hand, inspired by the experiments on imaging molecular orbitals using laser-induced electron tunneling and diffraction [32] controlled rescattering collisions can serve for the imaging of ultracold many-body wavefunctions.

Strong-field approximation. In the widely used strong-field approximation (SFA) [25, 33, 34] bound states of the potential other than the initial state are neglected and the final continuum state is replaced by a Volkov state, i.e. the solution of a free electron in a laser field. Therefore, the interaction of the electron with the remaining ion is ignored in the final state. Thus, the SFA does not support rescattering as can also be seen in Figs. 2c and d. On the other hand, the direct electrons and atoms (up to $2U_p$) in the quasistatic regime in Figs. 2c and d are qualitatively well described by the SFA. Similarly, the SFA reproduces the multi-peak structure in the multiphoton regime, see Figs. 2a and b. Note, the SFA is not gauge invariant and so far no arguments from first principles are known what gauge is to be preferred in which situation [35] (the gauge problem of SFA). In the simulator system, the number of trap states as well as the potential range can be varied which allows for an analysis of the assumptions and the gauge ambiguity of the SFA.

Interestingly, the SFA in velocity gauge allows to obtain the momentum density of the initial state since the energy-resolved yield is a product of the momentum-space density $|\tilde{\psi}(\mathbf{p})|^2$ and a prefactor $|g(\mathbf{p})|^2$ [24]. For a given momentum \mathbf{p} , the prefactor $g(\mathbf{p})$ depends solely on the vector potential $\mathcal{A}(t)$ and the binding energy. In contrast to the corresponding strong-field experiments, these parameters are known precisely for the quantum simulator because of the exactly known pulse shape. Note, this imaging technique relies on the agreement of the SFA in velocity gauge with the full TDSE results, which is fulfilled as seen in Figs. 2a and c despite the fact that the simulator mapping (5) is bound to the length gauge. Thus, this imaging technique indeed allows to image the momentum density of an ultracold gas in a trap.

Conclusion. A proposal for a quantum simulator for attosecond physics is presented based on ultracold atoms in an optical trapping potential. The simulator idea

connects the very contrary physics of ultracold, trapped atomic gases and the one of atoms, ions, and molecules in ultra-intense, ultra-short laser fields. The constraints one faces in strong-field experiments, such as the limitation to a specific molecular geometry, a fixed number of electrons per element or molecule, fixed interaction strengths, and limited pulse shapes are overcome in the simulator system. Moreover, the simulation can even reach parameter regions which are beyond those nowadays realizable in strong-field experiments, including, e.g., exotic pulse shapes and effective pulse durations corresponding to the sub-attosecond regime. In fact, the here proposed attosecond science in slow motion may shed light onto the ongoing debate on tunneling times [30, 36–38]. The numerical analysis of the here proposed concrete experimental realization of the quantum simulator with realistic experimental parameters demonstrates that it reproduces in its simplest configuration the ionization characteristics of a hydrogen atom. While this simple demonstrating example can be evaluated computationally, the simulator paves the way to systematically investigate many-body systems where the full numerical treatment is beyond the reach of any classical computer. Also the physics of ultracold atoms may profit from the quantum simulator by adopting concepts developed in attosecond science.

The authors gratefully acknowledge Selim Jochim, Gerhard Zürn, Thomas Lompe and Andre N. Wenz for valuable discussions and details of their experiment, and financial support from the *Studienstiftung des deutschen Volkes*, *Fonds der Chemischen Industrie*, and the *EU Initial Training Network (ITN) CORINF*.

-
- [1] R. P. Feynman, International Journal of Theoretical Physics **21**, 467 (1982).
 - [2] M. P. A. Fisher, P. B. Weichman, G. Grinstein, and D. S. Fisher, Phys. Rev. B **40**, 546 (1989).
 - [3] D. Jaksch, C. Bruder, J. I. Cirac, C. W. Gardiner, and P. Zoller, Phys. Rev. Lett. **81**, 3108 (1998).
 - [4] M. Greiner, O. Mandel, T. Esslinger, T. Hänsch, and I. Bloch, Nature **415**, 39 (2002).
 - [5] T. Stöferle, H. Moritz, C. Schori, M. Köhl, and T. Esslinger, Phys. Rev. Lett. **92**, 130403 (2004).
 - [6] M. Endres, T. Fukuhara, D. Pekker, M. Cheneau, P. Schauss, C. Gross, E. Demler, S. Kuhr, and I. Bloch, Nature **487**, 454 (2012).
 - [7] U. Schneider, L. Hackermüller, S. Will, T. Best, I. Bloch, T. A. Costi, R. W. Helmes, D. Rasch, and A. Rosch, Science **322**, 1520 (2008).
 - [8] R. Gerritsma, G. Kirchmair, F. Zähringer, E. Solano, R. Blatt, and C. F. Roos, Nature **463**, 68 (2010).
 - [9] S. Arlinghaus and M. Holthaus, Phys. Rev. A **81**, 063612 (2010).
 - [10] P. B. Corkum and F. Krausz, Nat. Phys. **3**, 381 (2007).
 - [11] P. M. Paul, E. S. Toma, P. Breger, G. Mullot, F. Augé, P. Balcou, H. G. Muller, and P. Agostini, Science **292**,

- 1689 (2001).
- [12] S. Haessler, J. Caillat, W. Boutu, C. Giovanetti-Teixeira, T. Ruchon, T. Auguste, Z. Diveki, P. Breger, A. Maquet, B. Carré, R. Taïeb, and P. Salières, *Nat. Phys.* **6**, 200 (2010).
- [13] J. Itatani, J. Levesque, D. Zeidler, H. Niikura, H. Pépin, J. C. Kieffer, P. B. Corkum, and D. M. Villeneuve, *Nature* **432**, 867 (2004).
- [14] Y. V. Vanne and A. Saenz, *Phys. Rev. A* **82**, 011403 (2010).
- [15] E. Dehghanian, A. D. Bandrauk, and G. L. Kamta, *Phys. Rev. A* **81**, 061403 (2010).
- [16] G. S. J. Armstrong, J. S. Parker, and K. T. Taylor, *New J. Phys.* **13**, 013024 (2011).
- [17] R. E. F. Silva, P. Rivière, and F. Martín, *Phys. Rev. A* **85**, 063414 (2012).
- [18] A. Palacios, H. Bachau, and F. Martín, *Phys. Rev. Lett.* **96**, 143001 (2006).
- [19] R. E. F. Silva, F. Catoire, P. Rivière, H. Bachau, and F. Martín, *Phys. Rev. Lett.* **110**, 113001 (2013).
- [20] D. B. Milošević, G. G. Paulus, D. Bauer, and W. Becker, *J. Phys. B* **39**, R203 (2006).
- [21] F. Serwane, G. Zürn, T. Lompe, T. B. Ottenstein, A. N. Wenz, and S. Jochim, *Science* **332**, 336 (2011).
- [22] C. Weitenberg, M. Endres, J. F. Sherson, M. Cheneau, P. Schausz, T. Fukuhara, I. Bloch, and S. Kuhr, *Nature* **471**, 319 (2011).
- [23] A. Saenz, *J. Phys. B* **33**, 4365 (2000).
- [24] See supplemental material for details.
- [25] L. V. Keldysh, *Sov. Phys. JETP* **20**, 1307 (1965).
- [26] S. Jochim and G. Zürn, private communication.
- [27] P. B. Corkum, *Phys. Rev. Lett.* **71**, 1994 (1993).
- [28] K. J. Schafer, B. Yang, L. F. DiMauro, and K. C. Kulander, *Phys. Rev. Lett.* **70**, 1599 (1993).
- [29] G. G. Paulus, W. Becker, W. Nicklich, and H. Walther, *J. Phys. B* **27**, L703 (1994).
- [30] D. Shafir, H. Soifer, B. D. Bruner, M. Dagan, Y. Mairesse, S. Patchkovskii, M. Y. Ivanov, O. Smirnova, and N. Dudovich, *Nature* **485**, 343 (2012).
- [31] B. Bergues, M. Kübel, N. G. Johnson, B. Fischer, N. Camus, K. J. Betsch, O. Herrwerth, A. Senftleben, A. M. Sayler, T. Rathje, T. Pfeifer, I. Ben-Itzhak, R. R. Jones, G. G. Paulus, F. Krausz, R. Moshhammer, J. Ullrich, and M. F. Kling, *Nat. Commun.* **3**, 813 (2012).
- [32] M. Meckel, D. Comtois, D. Zeidler, A. Staudte, D. Pavičić, H. C. Bandulet, H. Pépin, J. C. Kieffer, R. Dörner, D. M. Villeneuve, and P. B. Corkum, *Science* **320**, 1478 (2008).
- [33] F. H. M. Faisal, *J. Phys. B* **6**, L89 (1973).
- [34] H. R. Reiss, *Phys. Rev. A* **22**, 1786 (1980).
- [35] Y. V. Vanne and A. Saenz, *Phys. Rev. A* **79**, 023421 (2009).
- [36] M. Uiberacker, T. Uphues, M. Schultze, A. J. Verhoef, V. Yakovlev, M. F. Kling, J. Rauschenberger, N. M. Kabachnik, H. Schröder, M. Lezius, K. L. Kompa, H.-G. Muller, M. J. J. Vrakking, S. Hendel, U. Kleineberg, U. Heinzmann, M. Drescher, and F. Krausz, *Nature* **446**, 627 (2007).
- [37] A. N. Pfeiffer, C. Cirelli, M. Smolarski, D. Dimitrovski, M. Abu-samha, L. B. Madsen, and U. Keller, *Nat. Phys.* **8**, 76 (2012).
- [38] P. Eckle, A. N. Pfeiffer, C. Cirelli, A. Staudte, R. Dörner, H. G. Muller, M. Büttiker, and U. Keller, *Science* **322**, 1525 (2008).
- [39] G. Zürn, F. Serwane, T. Lompe, A. N. Wenz, M. G. Ries, J. E. Bohn, and S. Jochim, *Phys. Rev. Lett.* **108**, 075303 (2012).
- [40] F. Serwane, PhD thesis, University of Heidelberg (2011).
- [41] J. Förster, A. Saenz, and U. Wolff, *Phys. Rev. E* **86**, 016701 (2012).
- [42] Y. V. Vanne and A. Saenz, *J. Mod. Opt.* **55**, 2665 (2008).

SUPPLEMENTAL MATERIAL

Experimental parameters

The proposed experimental realization of the quantum simulator is based on the extension of an existing experiment. In the experiment [21], the potential of a tight optical dipole trap is populated with a degenerate Fermi gas consisting of ${}^6\text{Li}$ atoms in two hyperfine states. By applying a *static* magnetic-field gradient and varying the trap depth the atoms tunnel out of the trap in a fully controlled way, ending up with a defined number of particles in a determined quantum state. The experimental dipole trap is described in good approximation by a Gaussian-beam potential which results in a quasi 1D confinement with an aspect ratio of about 1:10. The beam profile in the longitudinal direction is approximately given by the Lorentz potential

$$\mathcal{V}_L(z) = \alpha \mathcal{V}_0 \left[1 - \frac{1}{1 + (z/z_r)^2} \right] . \quad (10)$$

Here, α is a modulation factor which allows to vary the trap depth in the experiment, see [21, 39], $\mathcal{V}_0/k_b = 3.33 \mu\text{K}$ is the potential depth, k_b the Boltzmann constant, $z_r = \pi w_0^2/\lambda$ the Rayleigh length with a laser wavelength of $\lambda = 1064 \text{ nm}$. In the experiment, the value of the waist w_0 has been $1.8 \mu\text{m}$. Achieving values lower than this is challenging but in principle a value of at least $w_0 = 0.7 \mu\text{m}$ could be realized with a new experimental setup [26, 40]. Here we chose $w_0 = 0.6 \mu\text{m}$. Moreover, we chose a realistic value for the trapping depth $\alpha = 0.02$. Certainly with the chosen Lorentz potential the long-range interaction of the nuclei and the electrons cannot be reproduced exactly. However, the choice of the parameters are such that energetic distribution of the low-lying bound-states resemble appropriately those of a 1D hydrogen atom with

$$V(z) = -\frac{1}{\sqrt{2+z^2}} . \quad (11)$$

On the other hand, systems with smaller binding potentials, like, e.g., anions, could be simulated more accurately. For anions, the long-range interaction of an emitted electron with the remaining neutral atom scales as $1/r^4$. This is more comparable to the long range interatomic interaction which scales like $1/r^6$ for neutral atoms or with $1/r^3$ for dipolar atoms.

Parameter mapping

For the simulator system natural units (n.u.) are introduced in which \hbar , the magnetic moment μ , the atomic mass m_a and the trap length d , which is equal to the extension of the ground-state wave function (defined as

the distance where the ground-state wavefunction has decreased to $1/e$ of its maximum value), are set to unity. It should be emphasized that different to atomic units (a.u.) which are uniquely defined to reflect the electronic properties of the hydrogen atom, the introduced natural units change with the trapping potential.

For a given simulator setup and a specific pulse, the corresponding values for the frequency ω_e and peak vector potential $|\mathbf{A}_0|$ applied in the strong-field system are found by enforcing equal Keldysh parameters

$$\gamma_e := \omega_e \frac{\sqrt{2m_e I_p}}{e E_0} = \omega \frac{\sqrt{2m_a E_b}}{\mu \mathcal{B}'_0} =: \gamma_a \quad (12)$$

and equal parameters

$$\beta_e := \frac{I_p}{\hbar \omega_e} = \frac{E_b}{\hbar \omega} =: \beta_a . \quad (13)$$

Here, I_p and E_b are the binding energies of the ground state of the field-free Hamiltonians (1) and (3) in the main manuscript, respectively. This mapping is not unique since E_b , which is determined by the shape of the trapping potential, is a free parameter. This freedom can be used to better adjust the trapping potential such that the energy-level distribution of the simulated system is resembled accurately.

In the manuscript, the considered pulses are defined via the vector potential although the simulator mapping is performed in length gauge. Since the simulator system is directly compared to the corresponding strong-field system, this is a convenient way to ensure that the pulse fulfills the zero net-force condition, i. e. the total integral over its electric (or magnetic) field is zero and the vector potential has the same value before and after the pulse.

Solution of the TDSE

The TDSE

$$i \frac{\partial}{\partial t} |\psi(t)\rangle = \hat{H} |\psi(t)\rangle \quad (14)$$

for the Hamiltonians \hat{H} and $\hat{\mathcal{H}}$, (1) and (3) in the main manuscript, respectively, are solved by expanding the wavefunction $|\psi(t)\rangle$ in eigenstates $|\phi\rangle$ of the field-free Hamiltonians \hat{H}_0 and $\hat{\mathcal{H}}_0$, (2) and (4) in the main manuscript, respectively.

While the finally shown spectra have been calculated within velocity gauge, i. e. equations (7) and (8) in the main manuscript, to achieve faster convergence, it was verified for a selected number of laser parameters that length and velocity gauge results are in full agreement.

The simulator system is treated numerically in one dimension. This approximation is well satisfied for the

here considered experimental realization since for ultra-cold temperatures the transversal motion of a strongly anisotropic trapping potential as realized in [21] is frozen out to the ground state.

For the solution of the 1D simulator [soft-Coulomb] system, the eigenstates of the field-free Hamiltonian are calculated via the matrix algorithm [41]. The results shown in the manuscript were obtained with a box size of $x_{\max} = 1200$ n.u. [$x_{\max} = 1200$ a.u.] and a grid consisting of 4001 [4201] points. For the time propagation, only 3001 [2001] states were used.

For the time propagation of the hydrogen atom, the field-free eigenstates are obtained in spherical coordinates (r, θ, φ) by expanding the radial problem in B splines (as in [42]). The results shown in the manuscript were obtained with a box size of $r_{\max} = 2000$ a.u. including states with angular momenta up to $l = 50$. Along the radial coordinate 4000 B splines of order 12 and a linear knot sequence were used. For the time propagation, only states with energies up to 10 a.u. above the ionisation threshold were considered.

Convergence of all spectra shown in the manuscript was ensured by varying the basis.

SFA in the simulator system

In analogy to the TDSE, the direct SFA ionization amplitude $\mathcal{M}_{\mathbf{p}}$ is easily translated from the corresponding

formula for the strong-field amplitude [20] applying equations (5) and (6) in the main manuscript. In length gauge it reads

$$\mathcal{M}_{\mathbf{p}}^{\text{LG}} = -i \int_0^{t_f} dt \langle \psi^V(t) | \mathbf{r} \cdot \mathbf{B}'(t) | \phi_0(t) \rangle \quad (15)$$

$$= \int_0^{t_f} dt e^{iS_{\mathbf{p}}(t)} \mathbf{B}'(t) \frac{d}{d\boldsymbol{\pi}(t)} \tilde{\phi}(\boldsymbol{\pi}(t)) \quad , \quad (16)$$

where $\boldsymbol{\pi}(t) = \mathbf{p} + \mathcal{A}(t)$, $S_{\mathbf{p}}(t) = E_b t + \frac{1}{2} \int_0^t d\tau \boldsymbol{\pi}(\tau)^2$ is the classical action, $\mathcal{A}(t)$ is the vector potential according to the mapping (6) in the main manuscript, $\tilde{\phi}$ is the Fourier transform of the initial state wavefunction, and $|\psi^V\rangle$ is the Volkov wavefunction. In velocity gauge, the amplitude is

$$\mathcal{M}_{\mathbf{p}}^{\text{VG}} = -i \tilde{\phi}(\mathbf{p}) \int_0^{t_f} dt e^{iS_{\mathbf{p}}(t)} \left(\mathbf{p} \cdot \mathcal{A}(t) + \frac{1}{2} \mathcal{A}(t)^2 \right) \quad (17)$$

and thus the yield

$$Y = |\mathcal{M}_{\mathbf{p}}^{\text{VG}}|^2 \equiv |\tilde{\phi}(\mathbf{p})|^2 |g(\mathbf{p})|^2 \quad (18)$$

contains the momentum-space density $\tilde{\phi}$ as a factor. This provides a way to extract the momentum-space density of the initial state from the measured energy-resolved spectra. In the limit of an infinite pulse, the integral even simplifies to an expression including generalized Bessel-functions [33].